課題番号　2012A—E32

重ね合わせガウスビームを用いたフェムト秒パルス誘起フィラメントの伝搬特性

Propagation characteristics of femtosecond filamentation
using a superposed Gaussian beam

秦　瑀[1)]　　板倉　隆二[2)]　　中嶋　隆[1)]

Yu　QIN　　Ryuji　ITAKURA　　Takashi　NAKAJIMA

[1)]京都大学　　[2)]原子力機構

Initially we planned to superpose two Gaussian beams with different diameters and investigate its propagation property. However, the superposed beam shows a severe power fluctuation due to the interference which could not be maintained stable for technical reasons. Therefore, we slightly changed our aim to the study of the propagation dynamics of different beam modes in dye solution (0.13% g/g, coumarin in methanol). During the experiment, beams with different modes, i.e., Gaussian or Bessel modes with different beam quality, are employed before sending the laser output into the liquid cell by using either a standard spherical lens or conical lens (so-called axicon lens). For each incident beam, the beam profile and spectrum are measured as a function of propagation distance and pulse energy. The images of fluorescence emission are taken from the side of the liquid cell as well. Compared with the Gaussian beam, the Bessel beam generated by the axicon lens shows an almost constant beam profile during the propagation. At the same time, the spectral broadening caused by the Bessel beam is found to be much less compared with that of the Gaussian beam with the similar peak intensity.

キーワード：femtosecond pulse; propagation; liquid; Gaussian beam; Bessel beam

１．目的

Due to the remarkable non-diffraction property, the Bessel beam may result in a high contrast filament along its long focal depth during nonlinear propagation [1-3]. To generate a Bessel beam, several methods have been used such as a circular slit combined with lens [4], or computer-generated holograms [5]. Recently, it has been found that the use of an axicon lens enables us to convert the Gaussian beam into the Bessel beam, which is technically very easy and efficient [6], and attracted considerable interests [7-11]. In this report, we will discuss two experiments on the femtosecond filamentation in liquid. In the first experiment we investigate the femtosecond filamentation by the high quality Gaussian and Bessel incident beams. In the second experiment we investigate the femtosecond filametation by the low, medium, and high quality Bessel beams which are, respectively, generated by sending the low, medium, and high quality Gaussian beams to the axicon lens for the mode conversion.

２．方法

Figure 1 shows the experimental setup. The laser pulse is from a Ti: Sapphire amplifier with ~mJ energy, 50 fs duration, and kHz repetition rate. The central wavelength is around 795 nm in the first experiment and 790 nm in the second experiment. The pulse energy can be easily controlled by rotating the half-wave plate. Incident beams to the liquid cell are prepared in different modes using different pinholes and spherical or axicon lens as we will describe later. The f=50 mm lens projects the magnified (4.2x) image of the propagating beam pattern on a slide glass onto the beam profiler. The elements in the dash boxes of Fig. 1 are put on an optical rail so that we can conveniently measure the beam profiles and spectra at different propagation distances. To monitor the on-axis laser intensity, we used a dye solution (0.13% g/g, coumarin in methanol) as a medium, and took the images of three-photon fluorescence by a camera.

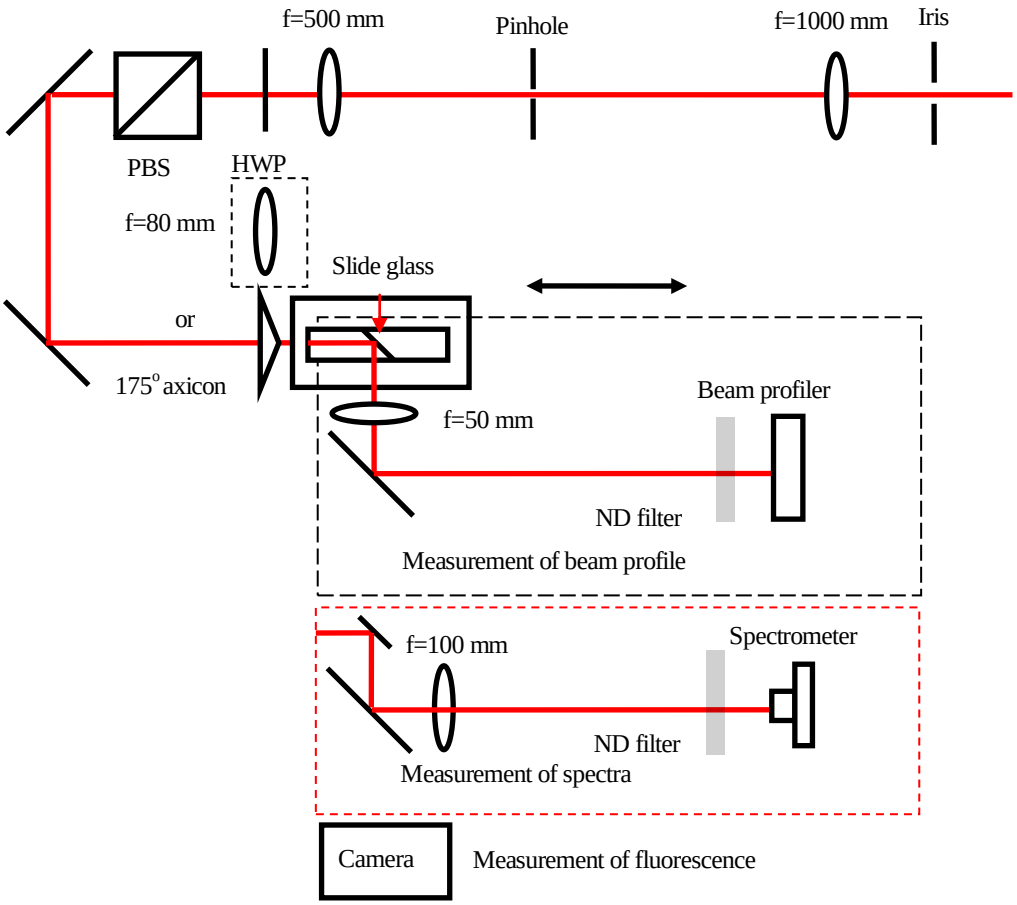

Fig.1. Experimental setup. PBS and HWP refer to a polarizing beam splitter and half-wave plate, respectively. Different detection systems shown in the dashed boxes are employed for different measurements.

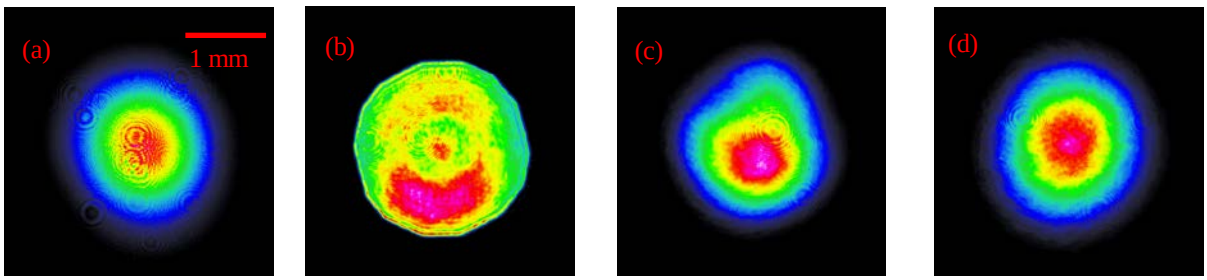

Fig. 2. Incident beam profiles used for the (a) first and (b)-(d) second experiments. In the first experiment, a high quality Gaussian beam as shown in panel (a) is focused into the liquid cell by the f=80 mm spherical lens or axicon lens with an apex angle of 175 °. In the second experiment, the inhomogeneous flat-top beam shown in panel (b) is spatially filtered by two different pinholes to result in Gaussian beams with different beam qualities as shown in panels (c) and (d).

The modes of the incident beams used for the first (Fig. 2(a)) and second (Figs. 2(b)-2(d)) experiments are shown in Fig. 2. In the first experiment, a high quality Gaussian beam is prepared by sending the laser output into the spatial filter, which further goes through a spherical or axicon lens to generate the Gaussian or Bessel modes. The spherical lens used here has a focus length of f=80 mm and results in the beam of ~15 μm diameter (FWHM) at the focus. The axicon lens used here has an apex angle of 175°, thus can generate a Bessel beam with a central width of ~15 μm diameter (FWHM). The distances between the lens and liquid surface are 15 mm for the axicon lens and 50 mm for the spherical lens, respectively. In the second experiment, only the axicon lens is used, while the incident beam quality before the axicon lens is controlled by the pinhole shown in Fig. 1. By inserting two different pinholes,

the inhomogeneous flat top beam (Fig. 2(b)) is converted to the Gaussian beams with different beam quality without changing the beam size too much (Figs. 2(c)-2(d)).

３．結果及び考察

3.1Filamentation by the Gaussian and Bessel incident beams

By measuring the beam profile, the self-focusing effect is observed for Gaussian beam at the energy as low as 1 μJ. However, for the Bessel beam, this does not happen when the energy changes from 3 to 33 μJ. Figure 3 shows the beam profiles of the Bessel beam at the different propagation distances for two different incident pulse energies. The beam modes and pulse energy are shown in the legend, where E is the incident pulse energy and z refers to the propagation distance in the liquid measured from the entrance window of the cell. From the figure, we can see that the Bessel beam keeps the same beam profile during the propagation at both pulse energies.

Figures 4(a) and 4(b) show the spectra for the Bessel incident beam at the different propagation distances with incident pulse energies of 3 and 33 μJ, respectively. The initial spectrum before the axicon

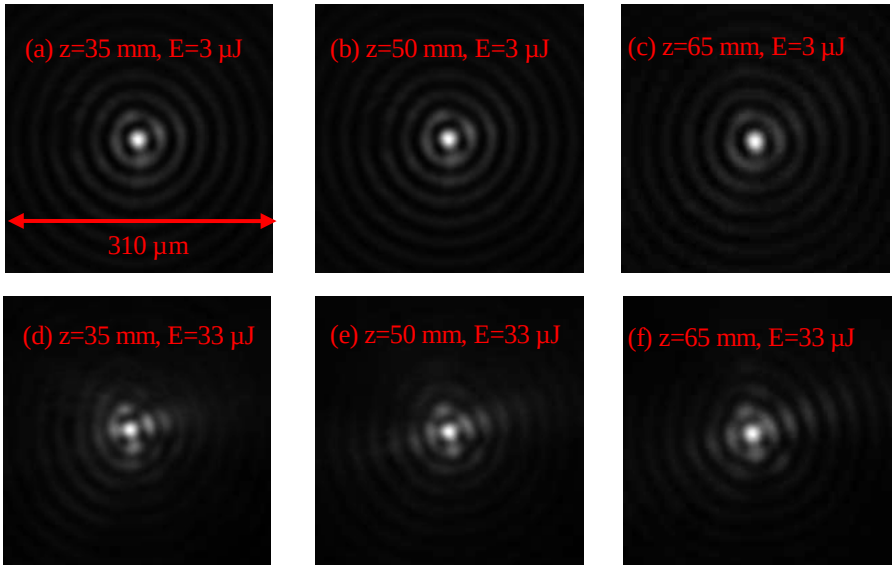

Fig. 3. Spatial evolution of the Bessel beam profiles at the different propagation distances, z= 30, 50, and 65 mm in liquid for the two different incident pulse energies, (a)-(c) 3 μJ and (d)-(f) 33 μJ.

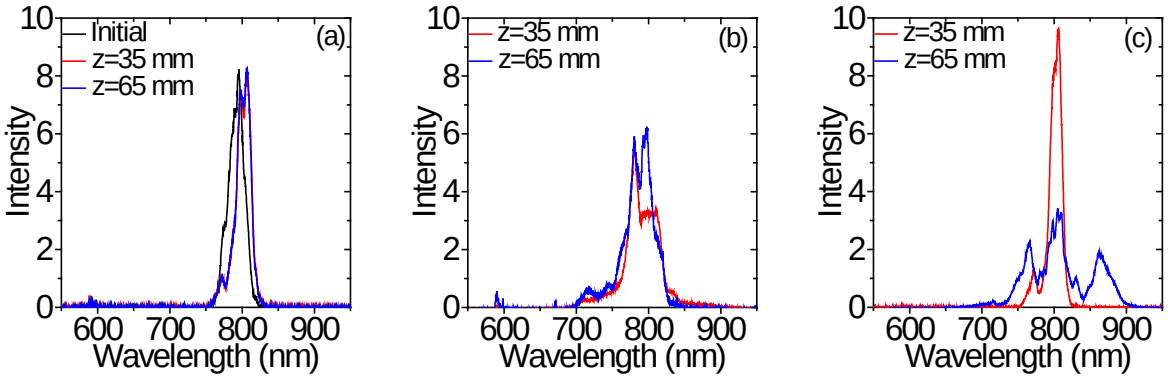

Fig. 4. (a) Spectra for the Bessel incident beam with 3 μJ pulse energy at the propagation distances of z=35 and 65 mm. (b) Similar to (a) but with 33 μJ pulse energy. (c) Similar to (a) but for the Gaussian incident beam with 2 μJ pulse energy.

lens is also shown in Fig. 4(a). The Gaussian beam with 2 μJ incident pulse energy generates the similar on-axis intensity with that of the 33 μJ Bessel incident beam at z=40 mm. For comparison, the spectra for the Gaussian incident beam with 2 μJ pulse energy at z=35 and 65 mm are shown in Fig. 4(c). Note that all the spectra in Fig. 4 have been normalized by the spectral intensity integrated over frequency.

For the Bessel incident beam with 3 μJ pulse energy the central wavelength is shifted to the longer wavelength side after the propagation in liquid, but the spectral broadening is very marginal, while for the 33 μJ Bessel incident beam the spectral broadening is significant. This broadening must be due to the self-phase modulation (SPM). However, the spectral widths are almost the same for both z=35 and 65 mm in each Figs. 4(a) and 4(b), which suggests that the spectral broadening is already completed before z=35 mm. For the case of the Gaussian incident beam with 2 μJ pulse energy (Fig. 4(c)), the gradual spectral broadening is observed during the propagation. Moreover, compared with the case of the Bessel incident beam with 33 μJ pulse energy in which the peak intensity of the central peak is similar to that of the Gaussian incident beam with 2 μJ pulse energy, the use of the latter incident beam results in a much broader spectrum at z=65 mm. This is not what we expected for the Bessel beam. The possible reason for this would be that the wave front of the Gaussian beam is almost plane at the beam waist, while the opening angle for the cone of the Bessel beam is around 15 mrad. Because of this large opening cone angle, the SPM may have been suppressed for the Bessel incident beam.

To compare the on-axis laser intensities by the Bessel and Gaussian incident beams, we show in Fig. 5 the images of the three-photon fluorescence emission of the dye solution for the Bessel incident beam with 33μJ pulse energy (Fig. 5(a)), Gaussian incident beam with 2 μJ pulse energy (Fig. 5(b)), Bessel incident beam with 15 μJ pulse energy (Fig. 5(c)), and Gaussian incident beam with 15 μJ pulse energy (Fig. 5(d)). From Figs. 5(a)-5(b), we find that the 33 μJ Bessel beam can keep a relatively high intensity for a much longer distance, although the intensity at z=40-45 mm is similar for both cases. Figures 5(c)-5(d) suggest that, given the same energy (15 μJ), the Gaussian beam generates much higher on-axis intensity, but the Bessel beam still shows a longer focal depth.

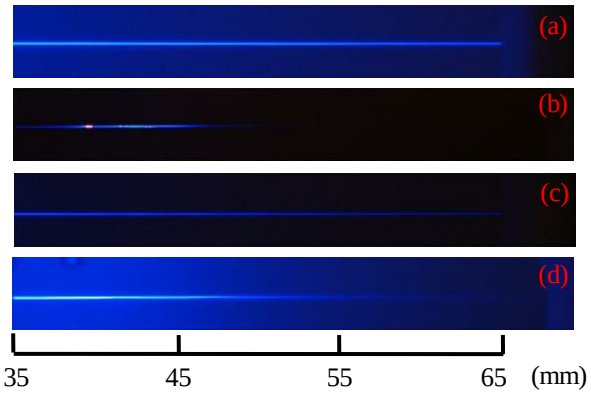

Fig. 5. Fluorescence images of the dye solution for the (a) Bessel incident beam with 33 μJ pulse energy, (b) Gaussian incident beam with 2 μJ pulse energy, (c) Bessel incident beam with 15μJ pulse energy, and (d) Gaussian incident beam with 15 μJ pulse energy.

3.2 Filamentation by the Bessel incident beams with different beam quality

In this section, we compare the filamentaiton by the Bessel incident beams with different beam quality produced by different pinholes. The three different beam profiles used to generate the Bessel beams before the axicon lens are shown in Figs. 1(b)-1(d). Namely, we use three different quality of the Gaussian beams to send them into the axicon lens to generate the Bessel beams with different beam quality. For convenience, we call them cases 1-3, respectively. Figure 6 summarizes the beam profiles at the different propagation distances for cases 1-3. For all three cases the incident pulse energy to the axicon lens has been fixed to 5 μJ. Figure 7 shows the similar data, but with the incident pulse energy to the axicon lens increased to 38 μJ. Compared with beam profiles of the Bessel beam produced in a similar way but with better spatially filtered as shown in Fig. 3, the beam quality of the Bessel beam in Fig. 6 looks worse. The possible reason is that the initial beam profiles are not as good as that in the previous experiment. But from Fig. 6, we can still find that compared with the inhomogeneous flat top beam (case1) and the Gaussian beam with low beam quality (case 2), the Gaussian beam with high beam quality (case 3) produces a Bessel beam with better quality. Besides, for case 3, the change of the beam profile during the propagation is much less.

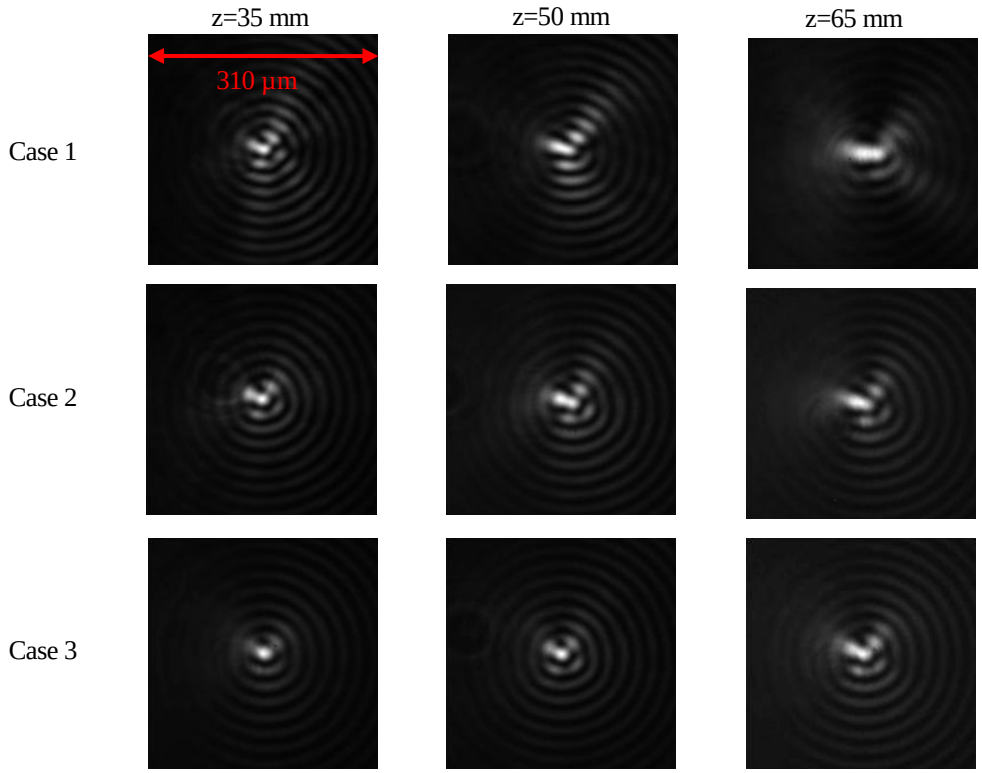

Fig. 6. Change of the beam profiles during propagation for the Bessel incident beams with different beam quality. Cases 1,2, and 3 correspond to the incident beam profiles shown in Figs. 1(b)-1(d), respectiverly, before the axicon lens. The incident pulse energy is fixed to 5 μJ for all three cases.

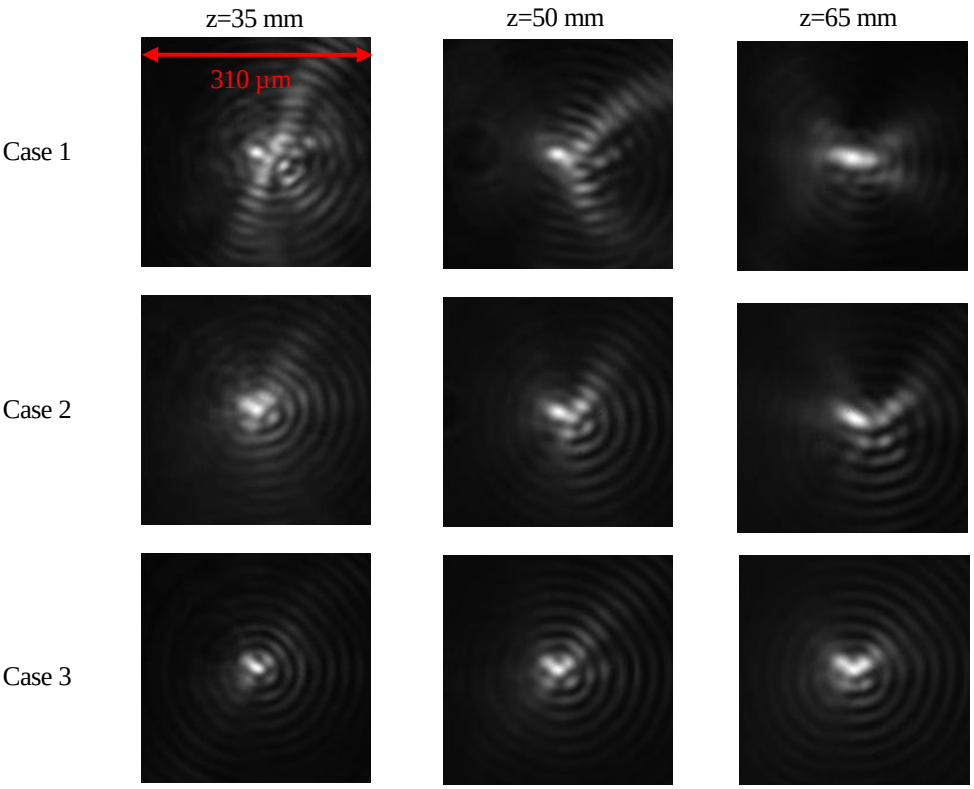

Fig. 7. Similar to Fig. 6 but with the incident pulse energy increased to 38 μJ.

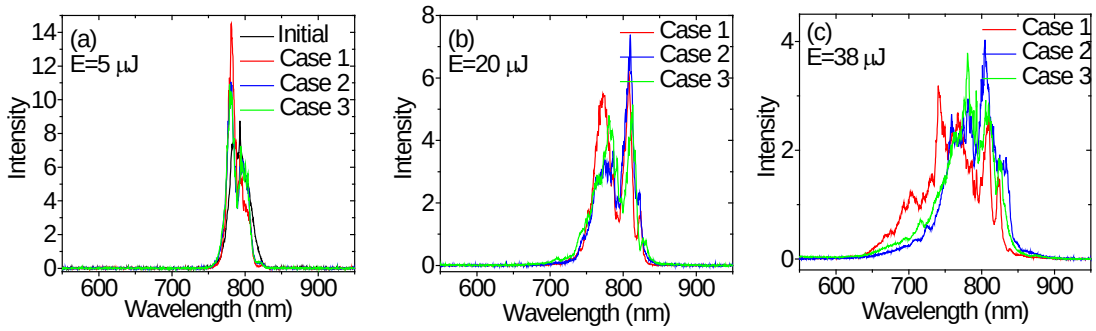

Fig. 8. Spectra at z=65 mm for the different beam quality of the Bessel incident beams which are generated by sending the beams shown in Fig. 1(b)-1(d), which are named as cases 1-3, into the axicon lens. The pulse energies of the Bessel beams are (a) 5 μJ, (b) 20 μJ, and (c) 38 μJ.

By comparing Figs. 6 and 7, we can see that, for case 3, the beam profile changes little when the energy increases, which is consistent with the previous experiment. For cases 1 and 2, the beam profiles are much more sensitive to the energy change.

Similar to the first experiment, the gradual spectral change over the propagation distance is not observed in the range of z=35-65mm. The spectra taken at z=65 mm for the different beam modes and energies are shown in Fig. 8 where the pulse energy and beam modes are given in the legend. Note that Figs. 8(a)-8(c) are plotted under the different vertical scales. The wavelength shift is also observed at the lower pulse energy (Fig. 8(a)). However, this time the shift is to the shorter wavelength side. At the higher pulse energies (Figs. 8(b)-8(c)), the spectral broadening is observed and the spectra for case 2 are very similar with those for case 3. But for case 1, more energy is contained in the shorter wavelength components as we see in Figs. 8(b) and 8(c). Interestingly with the incident energy of 38 μJ, the spectral broadening by the flat top beam (case 1) is the largest among cases 1-3. This is caused by the higher on-axis laser intensity for case 1, which will be shown later.

To know the on-axis laser intensity for cases 1-3, the images of the fluorescence emission have been converted to the numbers. After subtracting the background, the maximum values are picked at different propagation distances. The results are shown in Fig. 9 with the incident pulse energies of 5 μJ (Fig. 9(a)), 20 μJ (Fig. 9(b)) and 38 μJ (Fig. 9(c)). The on-axis laser intensities and nearly equivalently the fluorescence intensities are very similar for cases 2 and 3. But for case 1, the intensity is much higher, and shows a plateau during which the intensity decreases at a much lower rate as the pulse propagates. This plateau structure seems to be more extended when the pulse energy increases.

In summary, we have experimentally demonstrated that the Bessel beam can be generated by focusing the Gaussian beam with an axicon lens. This Bessel beam keeps a constant beam profile during the propagation. Compared with the Gaussian incident beam, the spectral broadening generated by the Bessel incident beam is much weaker for the same beam diameter and peak intensity. We have also confirmed that the Gaussian beam with a good spatial quality through a spatial filter must be employed to generate a

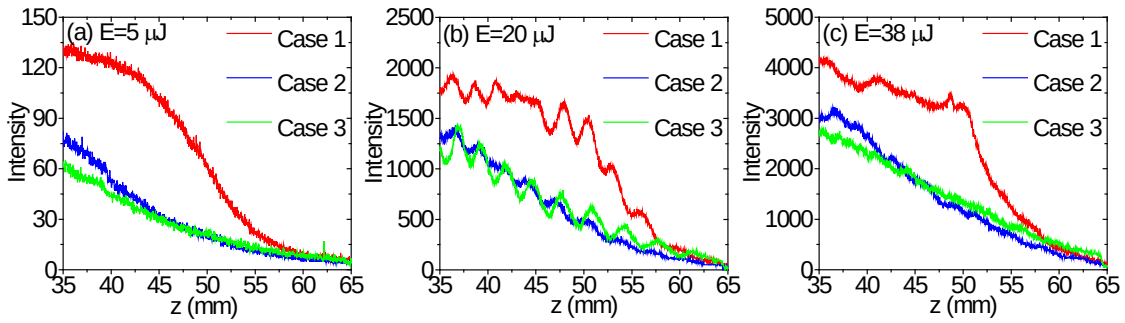

Fig.9. On-axis fluorescence intensity for the three different incident beam modes, cases 1-3. The pulse energies are (a) 5 μJ, (b) 20 μJ, and (c) 38 μJ, respectively.

Bessel beam with good beam quality by the mode conversion with an axicon lens, otherwise the beam mode after the axicon lens exhibits strong distortions and loses an annular structure of the Bessel beam.

４．引用(参照)文献等

1. Z. Song, Z. Zhang, and T. Nakajima, Opt. Express **17**, 12217 (2009).
2. Z. Song and T. Nakajima, Opt. Express **18**, 12923 (2010).
3. P. Polesana, M. Franco, A. Couairon, D. Faccio, and P. Di Trapani, Phys. Rev. A **77**, 043814 (2008).
4. J. E. Durnin, J. J. Miceli, and J. H. Eberly, Phys. Rev. Lett. **58**, 1499 (1987).
5. A. Vasara, J. Turunen, and A. T. Friberg, J. Opt. Soc. Am. **6**, 1748 (1989).
6. M.-D. Wei, W.-L. Shiao, and Y.-T. Lin, Opt. Commun **248**, 7 (2005).
7. P. Polesana, A. Couairon, D. Faccio, A. Parola, M. A. Porras, A. Dubietis, A. Piskarskas, and P. Di Trapani, Phys. Rev. Lett. **99**, 223902 (2007).
8. P. Polynkin, M. Kolesik, A. Roberts, D. Faccio, P. Di Trapani, and J. Moloney, Opt. Express **16**, 15733 (2008).
9. S. Akturk, B. Zhou, M. Franco, A. Couairon, and A. Mysyrowicz, Opt. Commun. **282**, 129 (2009).
10. K. Dota, A. Pathak, J. A. Dharmadhikari, D. Mathur, and A.K. Dharmadhikari, Phys. Rev. A **86**, 023808 (2012)
11. Sun, H. Gao, S. Xu, W. Liu, Y. Cheng, Z. Xu, and G. Mu, Opt. Lett **37**, 857 (2012)